NJC

Aggregation behavior of group 12 complexes of a tripodal mixed NS(thiolato) donor ligand

Journal:	*New Journal of Chemistry*
Manuscript ID	NJ-ART-12-2023-005532.R1
Article Type:	Paper
Date Submitted by the Author:	05-Jan-2024
Complete List of Authors:	Sturner, Michelle; William & Mary, Department of Chemistry Thomas, Isla; William & Mary, Department of Chemistry Owusu-Koramoah, Joshua; William & Mary, Department of Chemistry Reynolds, Todd; William & Mary, Department of Chemistry Berry, Steven; William & Mary, Department of Chemistry; University of Minnesota Duluth, Department of Chemistry & Biochemistry Butcher, Raymond; Howard University, Bebout, Deborah; William & Mary, Department of Chemistry

ARTICLE

Aggregation behavior of group 12 complexes of a tripodal mixed NS(thiolato) donor ligand†‡

Received 00th January 20xx,
Accepted 00th January 20xx

DOI: 10.1039/x0xx00000x

Michelle A. Sturner,[a] Isla D. Thomas,[a] Joshua E. Owusu-Koramoah,[a] Todd M. Reynolds,[a] Steven M. Berry,[a,b] Raymond J. Butcher[c] and Deborah C. Bebout*[a]

Despite the concurrence of histidine and cysteine in the active sites of proteins associated with Zn^{2+}, Cd^{2+} and Hg^{2+}, coordination studies of these metal ions with chelating ligands containing a combination of aromatic amine and alkylthiolate ($N_x^AS_y^-$) donors have been rare. The potentially tetradentate ligand 2-[bis(2-pyridinylmethyl)amino]ethanethiol (**LH**) and chloride salts were used to prepare new complexes of Cd^{2+} and Hg^{2+} for comparison with the known Zn^{2+} complex. Solution NMR studies revealed concentration-dependent equilibria between aggregate forms of the new complexes in CD_3CN. Trends in homonuclear and heteronuclear coupling provided additional insight regarding solution equilibria. ESI-MS from acetonitrile solutions supported differences in preferred aggregation states consistent with the solution NMR studies.

Introduction

The distribution of amino acid side chain contacts in the Protein Data Bank suggests that Zn^{2+}, Cd^{2+}, and Hg^{2+} share a common preference for cysteine and histidine ligation.[1] Furthermore, these amino acids appear together in a variety of group 12 metal ion protein binding sites. For example, His_2Cys_2 zinc fingers are common protein structural components.[2] Evidence for histidine metal bonding has also recently been reported for several cysteine-rich metallothioneins, proteins with functions including zinc homeostasis as well as Cd^{2+} and Hg^{2+} detoxification.[3] Human proteins containing zinc centers with both histidine and cysteine side chain ligation occur in the catalytic sites of at least four enzyme classes (Table 1). Structural and regulatory Zn-Cys-His sites occur in at least five classes of mammalian enzymes (Table 2). Additional structurally characterized enzymes from non-mammalian organisms document Zn-Cys-His sites in isomerases and translocases.[4, 5] Significantly, the cambialistic ζ-class of carbonic anhydrases from marine diatoms relying on Cd^{2+} as their metal cofactor when Zn^{2+} is scarce have His_2Cys metal binding environments like the prokaryotic β-class of Zn^{2+}-dependent carbonic anhydrase instead of the His_3 environment associated with most Zn^{2+}-dependent classes.[6]

Despite the concurrence of histidine and cysteine in the active sites of proteins associated with stable group 12 metal ions, coordination studies of these metal ions with chelating ligands containing a combination of aromatic amine and alkylthiolate ($N_x^AS_y^-$) donors have been rare. A search of the Cambridge Crystallographic Database[7] reveals two Cd^{2+} complexes[8, 9] and one Hg^{2+} complex[10] incorporating chelating $N_x^AS_y^-$ ligands. Interestingly, a study inspired by the metal-promiscuity of metallothionein used a $N_x^AS_y^-$ ligand to provide the first crystallographically characterized complexes containing both Zn^{2+} and Hg^{2+} bound to the same ligand.[11] A very limited variety of bi-, tri- and tetradentate $N_x^AS_y^-$ ligands have been used to prepare structurally characterized Zn^{2+} complexes.[7] For context, additional potential structural models of molecular mixed histidine-cysteine protein group 12 metal ion bonding sites have been obtained with non-alkylthiolates including, for example, chelating 8-mercaptoquinalato ligands[12-19] or monodentate aryl thiolates combined with aromatic amine ligands.[20-28]

An interesting phenomenon with d^{10} metal ion complexes is their rapid exchange of low denticity ligands.[29, 30] This has implications for their bioreactivity, as well as their general coordination chemistry. The metal-bridging capabilities of thiolate donors adds another layer of complexity to the coordination number and geometry equilibria that plague the coordination chemistry of d^{10} metal ions. The tripodal ligand 2-[bis(2-pyridinylmethyl)amino]ethanethiol (**LH**; Fig. 1) was chosen for this study because it has supported preparation of

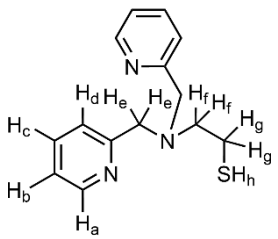

Figure 1. Structure of **LH** with proton labels.

[a] *Department of Chemistry, William & Mary, Williamsburg, VA, United States. Email: dcbebo@wm.edu*
[b] *Current address: Department of Chemistry & Biochemistry, University of Minnesota – Duluth, Duluth, MN, United States.*
[c] *Department of Chemistry, Howard University, Washington D.C., United States.*

†Dedicated to the corresponding author's inspiring Cornell University graduate advisor Barry Carpenter on the occasion of his recent retirement from Cardiff University.

‡Electronic Supplementary Information (ESI) available: Crystallization and characterization of additional solvates of **1**, packing diagrams, additional NMR and ESI-MS spectra. CCDC 2296073-4 and 2311421-2. For ESI and crystallographic data in CIF or other electronic format see DOI:10.1039/x0xx00000x

Table 1. Representative human enzymes containing catalytic Zn^{2+}-cysteine-histidine complexes.[a]

Enzyme Class	Protein	Zn^{2+}-sidechain interactions	PDB	Ref.
Oxidoreductase	Alcohol dehydrogenase	$Cys_{44}His_{66}Glu_{67}Cys_{173}$	1MA0	31
	Sorbitol dehydrogenase	$Cys_{44}His_{69}Glu_{70}$	1PL7	32
Transferase	Protein farnesyltransferase	$Asp_{297}Cys_{299}His_{362}$	1JCQ	33
Hydrolase	Cytidine deaminase	$His_{67}Glu_{69}Cys_{98}Cys_{101}$	2KEM	34
	GTP Cyclohydrolase I	$Cys_{141}Cys_{212}His_{144}$	1FB1	35
Ligase	Threonyl-tRNA Synthetase	$Cys_{413}His_{464}His_{590}$	4P3N	36

[a] Adapted from reference [37].

Table 2. Representative mammalian enzymes containing regulatory or structural Zn^{2+}-cysteine-histidine complexes.[a]

Enzyme Class	Protein	Organism [b]	Zn^{2+}-sidechain interactions	PDB	Ref
Oxidoreductase	Histone demethylase LSD2	H	$Cys_{53}Cys_{58}His_{84}His_{90}$	4FWE	31
Transferase	Bruton's tyrosine kinase	H	$His_{143}Cys_{154}Cys_{155}Cys_{165}$	1B55	38
	Protein kinase C	R	$His_{102}Cys_{135}Cys_{115}His_{140}$	3PFQ	39
	UDP-GlcNAc 2-epimerase/ ManNAc 6-kinase (GNE)	H	$His_{569}Cys_{579}Cys_{581}Cys_{586}$	3EO3	40
Hydrolase	Cathepsin S	H	$Cys_{25}His_{164}$	2HH5	41
	Dimethylarginine dimethylaminoydrolase	B	$His_{172}Cys_{273}$	2CI7	42
Lyase	Aprataxin and PNK-like factor	H	$Cys_{379}Cys_{385}His_{392}His_{398}$ $Cys_{421}Cys_{427}His_{434}His_{440}$	2KQB 2KQC	43
Ligase	RING-type E3 ubiquitin ligase	H	$Cys_{100}Cys_{103}His_{115}Cys_{119}$	5DKA	44

[a] Adapted from reference [37]; [b] B = *Bos taurus*; H = *Homo sapiens*; R = *Rattus norvegicus*.

mononuclear and binuclear models of cysteine- and histidine-containing protein metal binding sites. For example, the distorted trigonal bipyramidal complex [Zn**L**Cl] was found to promote metallo-β-lactamase-like hydrolysis activity.[45] However, the rate of bis(p-nitrophenyl)hydrogen phosphate hydrolysis increased linearly with [Zn**L**Cl] at low concentrations, then gradually decreased as higher concentration suggesting a monomer-dimer equilibrium. Adding methyl groups ortho to the pyridyl nitrogen of **LH** produced a similar mononuclear square pyramidal zinc complex.[46] In addition, a complex of **L** with a bis(μ-thiolato)dicopper(II) core resembles the Cu_A sites of cytochrome *c* oxidase and nitrous oxide reductase.[47] In this work, the syntheses, X-ray crystallography, ^{1}H NMR, and IR of [Cd**L**Cl]$_2$·benzene (**1**·benzene) and [Hg**L**Cl] (**2**) are described, completing the first series of structurally characterized group 12 complexes with a common chelating $N_x^A S_y^-$ ligand. Extensive solution NMR studies supplemented by ESI-MS studies document differences in aggregation behavior.

Experimental

Materials and methods.

Organic solvents and reagents were of commercial grade and used as received. Metal salts were dried under vacuum overnight. Elemental analyses were carried out by Atlantic Microlab, Inc., Norcross, Georgia. Capillary melting points were obtained using a Mel-Temp apparatus and are uncorrected. ^{1}H NMR spectra were collected in 5 mm o.d. NMR tubes on an Agilent 400MR DD2 NMR spectrometer. IR spectra were collected on a Digital Labs FTS 7000 using a diamond ATR probe.

Single crystal diffraction data were collected at 103 K using graphite-monochromated Mo Kα X-radiation (λ = 0.71073 Å) on a Bruker SMART 1000 (**1**·benzene) or Siemens P4 four-circle diffractometer (**2**). The structures were solved by direct methods and refined on F^2 by full-matrix least squares using the ShelXle 2019/3 program package.[48] All non-hydrogen atoms were refined anisotropically and the hydrogens were placed theoretically. Crystallographic data for **1**·benzene and **2** are provided in Table 3.

Mass Spectrometry experiments were carried out with a Finnigan LCQ XL electrospray ionization ion trap mass spectrometer. A capillary temperature of 100-200 ° C, an ion gauge pressure of 2.0×10^{-5} Torr, and a syringe pump flow rate of 10 μL/min were used for all samples. Ions were isolated with qz 0.250, activation time 30 ms, and sufficient mass width to collect isotopomers with greater than 1% predicted relative abundance. Isolated ions were subjected to collision-induced dissociation with the background helium atoms at varying activation energies. High resolution ZoomScan spectra were used to confirm ion charge states and collect isotopomer distributions for comparison to theoretical expectations.

Synthesis of LH. LH was synthesized and purified by literature methods.[45] ^{1}H NMR (CD_3CN, 20 °C): ^{1}H NMR ($CDCl_3$) δ 8.506 (d, 4 H, J = 5.0 Hz, H_a), 7.643 (dt, 4 H, J = 1.9, 7.8 Hz, H_c), 7.519 (d, 4 H, J = 7.8 Hz, H_d), 7.139 (d, 4 H, J = 5.3, 7.4 Hz, H_b), 3.829 (s, 4 H, H_e), 2.792 (m, 4 H, H_g), 2.652 (m, 4 H, H_f); (CD_3CN) δ 8.478 (d, 4 H, J = 5.1 Hz, H_a), 7.708 (dt, 4 H, J = 1.7, 7.8 Hz, H_c), 7.547 (d, 4

Table 3. Crystallographic data for 1·benzene and 2

	1·benzene	**2**
Empirical Formula	$C_{34}H_{38}Cd_2Cl_2N_6S_2$	$C_{14}H_{16}ClHgN_3S$
Formula mass [g mol^{-1}]	890.52	494.40
Crystal Size [mm^3]	0.30 × 0.45 × 0.58	0.12 × 0.48 × 0.48
Crystal System	Triclinic	Monoclinic
Space Group	*P*-1	$P2_1/c$
a[Å]	9.0044(9)	12.5678(13)
b[Å]	10.0424(10)	7.6751(8)
c[Å]	10.5406(10)	16.4006(18)
α[°]	75.097(2)	90
β[°]	72.253(2)	96.284
γ[°]	88.380(2)	90
V[Å^3]	875.95(15)	1572.5(3)
Z	1	4
Radiation (monochromatic)	Mo Kα	Mo Kα
T [K]	103(2)	103(2)
ρ_{calc} [Mg m^{-3}]	1.688	2.088
λ [Å]	0.71073	0.71073
μ [mm^{-1}]	1.520	10.083
Measured reflections	6814	11184
Ind. Reflections [$R_{(int)}$]	4134 [0.0303]	3746 [0.0423]
Completeness to θ = 25.242°	99.2 %	99.6%
Data/restraints/parameters	4134 / 0 / 209	3746 / 0 / 181
R1[a], wR2[b] [$I > 2\sigma(I)$]	0.0267, 0.0731	0.0275, 0.0578
R1[a], wR2[b] (all data)	0.0274, 0.0738	0.0324, 0.0593
Goodness-of-fit (GOF)	1.050	1.106

[a] $R_1 = \Sigma||F_o| - |F_c||/\Sigma|F_o|$, and $S = [\Sigma[w(F_o^2 - F_c^2)^2]/(n-p)]^{1/2}$; [b] $wR_2 = [\Sigma[w(F_o^2) - (F_c^2)]^2/\Sigma[w(F_o^2)^2]^{1/2}$

H, *J* = 7.7 Hz, H_d), 7.199 (d, 4 H, *J* = 4.9, 7.6 Hz, H_b), 3.784 (s, 4 H, H_e), 2.730 (m, 4 H, H_g), 2.648 (m, 4 H, H_f).

Crystallization of [CdLCl]$_2$·benzene (1·benzene). One equivalent of methanolic KOH (0.4 M, 790 µL, 316 µmol) was added to a solution of LH (82 mg, 316 µmol) in 4 mL methanol. A suspension of $CdCl_2$ (58 mg, 316 µmol) in 18 mL methanol was added with stirring. A homogeneous solution was obtained after stirring overnight. Benzene was added dropwise to the cloud point. The solution was filtered through Celite and set aside for slow evaporation. Colorless X-ray quality crystals (27 mg, 19% yield) formed in seven days. Crystals became opaque over time or if placed under vacuum. Similar methods led to isolation of m-xylene and methanol solvates (see supplemental information). MP: 232 – 235 °C. ^{1}H NMR (CD_3CN, saturated, 20 °C): δ 8.904 (d, 4 H, *J* = 4.9 Hz, H_a), 7.931 (ddd, 4 H, *J* = 1.7, 7.8, 7.8 Hz, H_c), 7.504 (dd, 4 H, *J* = 5.0, 7.6 Hz, H_b), 7.420 (d, 4 H, *J* = 6.8 Hz, H_d), 7.371 (s, 6 H, $H_{benzene}$), 3.999 (d, 4 H, *J* = 15.4 Hz, H_e), 3.749 (d, 4 H, *J* = 15.5 Hz, H_e'), 2.760-2.660 (m, 4 H, $H_{f,g}$). IR (ATR) ν/cm^{-1}: 617(w), 633(w), 646(w), 660(w), 689(s), 723(w),768(s),802 (w), 825(w), 845(w), 920(w), 935(w), 966(w), 988(w), 1011(m), 1036(w), 1051(w), 1096(m), 1121(w), 1150(m), 1217(w), 1260(w), 1275(w), 1292(w), 1304(w), 1348(w), 1389(w), 1431(m), 1458(w), 1476(m), 1572(w), 1595(m), 2342(w), 2363(w), 2843(w), 2909(w). Anal. Calc for vacuum dried (benzene lost) $Cd_2C_{28}H_{32}N_6S_2Cl_2$: 45.85 C, 4.30 H, 9.44 N. Found: 45.96 C, 4.28 H, 9.42 N.

Crystallization of [HgLCl] (2). One equivalent of $HgCl_2$ (63.8 mg, 235 µmol) in 3 mL methanol was added to solution of **LH** (60.9 mg, 235 µmol) in 1.5 mL acetonitrile and NaOH (0.4 M in methanol, 588 µL, 235 µmol). Triethylamine was added dropwise to the cloud point, followed by dropwise addition of acetonitrile to clarify. The solution was filtered through Celite and set aside. After seven days, the clear solution was carefully decanted from trace gray sediment and set aside for slow evaporation. Colorless X-ray quality crystals (62.2 mg, 53.5% yield) were obtained a week later. DP: 118 °C. ^{1}H NMR (CD_3CN, nominally 2 mM, 20 °C) δ: 8.873 (d, 2H, *J* = 5.0 Hz, H_a), 7.831 (ddd, 2H, *J* = 1.8, 7.7, 7.7 Hz, H_c), 7.417 (dd, 2H, *J* = 5.1, 8.2 Hz, H_b), 7.358 (d, 2H, J = 7.2 Hz, H_d), 3.810 (bs, 4H, H_e), 2.875 (bs, 2H, H_g), 2.695(m, 2H, H_f). IR (ATR) ν/cm^{-1}: 633(m), 644(w), 660(w), 687(w), 723(m), 760(s), 802(w), 837(w), 891(m), 912(w), 939(w), 962(w), 988(w), 1009(m), 1026(w), 1049(m), 1092(m), 1109(w), 1128(m), 1155(w), 1196(w), 1236(w), 1265(m), 1285(w), 1300(w), 1315(w), 1371(m), 1435(s), 1472(m), 1573(m), 1597(s), 2835(w), 2878(w), 2914(w), 2940(w), 3742(w), 3750(w), 3852(w). Anal. Calc for $HgC_{14}H_{16}N_3SCl$: 34.01 C, 3.26 H, 8.50 N. Found: 34.06 C, 3.22 H, 8.49 N.

Results and discussion

Syntheses of [CdLCl]$_2$·benzene and [HgLCl]

New compounds of Cd^{2+} and Hg^{2+} with the N_3S donor ligand **L**$^-$ were prepared by self-assembly in solutions containing one equivalent of **LH** per equivalent of metal chloride. Colorless crystals of [Cd**L**Cl]$_2$·benzene (**1**·benzene) were obtained in low yield from methanol by slow evaporation using benzene as a co-solvent. The complex had satisfactory elemental analysis allowing for the loss of benzene during vacuum drying. Colorless crystals of [Hg**L**Cl] (**2**) with satisfactory elemental analysis were obtained by slow evaporation using acetonitrile/methanol/triethylamine as co-solvents. Both compounds were characterized by single crystal X-ray diffraction, IR and variable temperature solution state ^{1}H NMR.

Structure of [CdLCl]$_2$·benzene

The neutral dinuclear complex [Cd**L**Cl]$_2$·benzene (**1**·benzene) crystallized in the triclinic space group *P*-1 with one dimeric complex and one well-ordered benzene molecule per unit cell. Both the complex and the benzene molecule lie on crystallographic inversion centers. As shown in Figure 2, each metal center has distorted octahedral ClN_3S_2 coordination

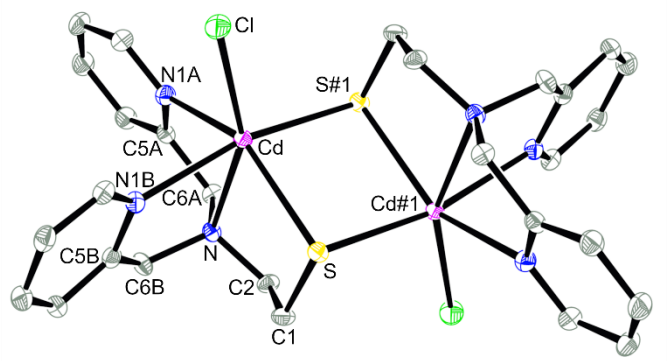

Figure 2. Thermal ellipsoid (50% probability) structure of the metal complex in **1**·benzene. Hydrogen atoms and benzene solvent are omitted for clarity.

provided by a tetradentate **L**, a terminal chloride and a bridging thiolate. The N1B pyridyl nitrogens are trans to chelating thiolate sulfurs and the N1A pyridyl nitrogens are trans to bridging thiolate sulfurs. Finally, the tertiary amine nitrogen and chloride are trans and located on either side of the plane containing the $(CdS)_2$ ring. Non-isomorphic solvomorphs **1**·m-xylene and **1**·MeOH (with ethyl acetate cosolvent) crystallized with comparable dinuclear complex structures (see supporting information).

The chelating Cd–S bond length (2.6777(5) Å) is slightly longer than the bridging Cd-S#1 (2.6449(6) Å) (Table 4). The average Cd–$N_{pyridyl}$ bond length is 2.4258(18) Å, somewhat

Table 4. Selected bond lengths and angles for $[MLCl]_n \cdot m$ benzene

M	Cd	Hg	Zn[45]
n, m	2, 1	1, 0	1, 0
M–N1A	2.4122(17)	2.510(4)	2.113(3)
M–N1B	2.4394(18)	2.480(3)	2.130(4)
M–N	2.4753(17)	2.644(3)	2.313(3)
M–S	2.6777(5)	2.4185(12)	2.303(1)
M–Cl	2.5264(6)	2.4591(11)	2.337(1)
M–S#1	2.6449(6)		
N1A–M–N1B	84.66(6)	103.22(12)	115.0(1)
N1A–M–N	68.76(6)	67.43(11)	75.6(1)
N1B–M–N	71.17(6)	66.65(11)	76.1(1)
N1A–M–Cl	91.85(4)	91.60(9)	98.6(1)
N1B–M–Cl	92.30(5)	93.22(9)	97.0(1)
N–M–Cl	155.12(4)	144.96(8)	167.59(9)
N1A–M–S	148.82(4)	110.88(9)	118.68(10)
N1B–M–S	85.14(4)	118.68(9)	116.0(1)
N–M–S	80.05(4)	81.47(8)	85.80(9)
Cl–M–S	117.952(18)	133.34(4)	106.57(5)
N1B–M–S#1	165.58(5)		
N1A–M–S#1	95.18(4)		
N–M–S#1	95.29(4)		
Cl–M–S#1	102.108(19)		
S–M–S#1	87.691(16)		
M–S–M#1	92.309(15)		

Symmetry code: #1 –x + 1, –y + 2, –z + 1

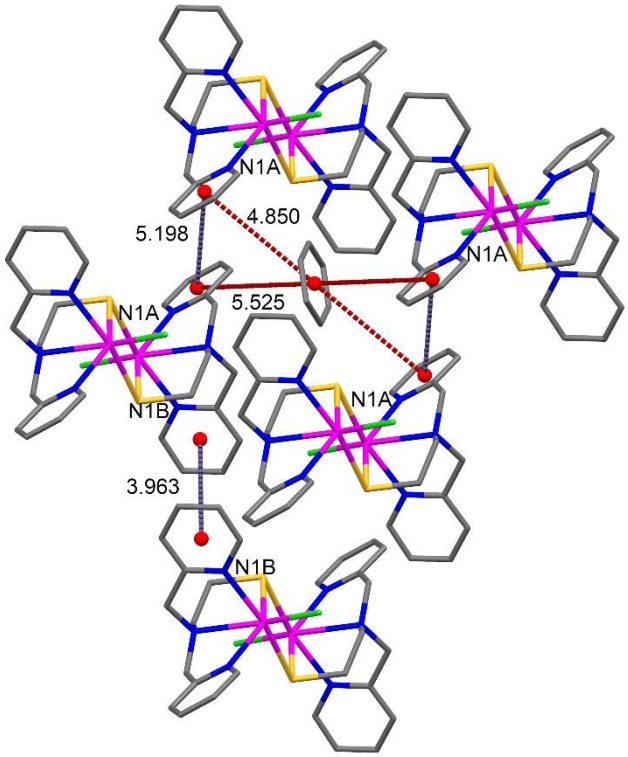

Figure 3. Intermolecular aromatic centroid distances (Å) between pyridyl rings identified by their nitrogen atom and benzene trapped in the crystal lattice of **1**·benzene. Hydrogen atoms are omitted for clarity. Offset parallel pyridyl-pyridyl centroid distances in violet; multimolecular embrace pyridyl-benzene centroid distances in red.

shorter than the Cd–N_{am} bond length (2.4753(17) Å) where N_{am} is the central ammine nitrogen atom of the tripodal ligand. The N1A/C5A/C6A/N, N1B/C5B/C6B/N and S/C1/C2/N chelate rings have distorted envelope conformations with atoms N, C6B and C2 in the flap positions, respectively. Geometric constraints of the tripodal ligand likely cause displacement of the metal ion from the N1A–N1B–S–S#1 plane towards the chloride, resulting in many distortions from regular octahedral geometry. In addition, torsional strain between substituents on the planar $(CdS)_2$ ring is moderated by the 155.12(4)° Cl–Cd–N bond angle.

The supramolecular structure of **1**·benzene is stabilized through synergistic aromatic interactions (Fig. 3).[49] The dimer complex is assembled into sheets through C–H π attractions[50] between pairs of N1A pyridyl rings and offset face-to-face π–π (OFF) interactions[51] between pairs of N1B pyridyl rings (Fig. S1). The lattice benzene is loosely held in place by a concerted multimolecular embrace[52] involving four neighboring N1A pyridyl rings (Fig. 3). Benzene placement in channels between sheets is consistent with ready solvent loss under vacuum (Fig. S1).

Structure of [HgLCl]

The neutral mononuclear complex [Hg**L**Cl] (**2**) crystallized in the monoclinic space group $P2_1/c$ with four molecules per unit cell. As shown in Figure 4, the metal ion has ClN_3S coordination. Complex **2** has mixed metal ion coordination geometry (τ =

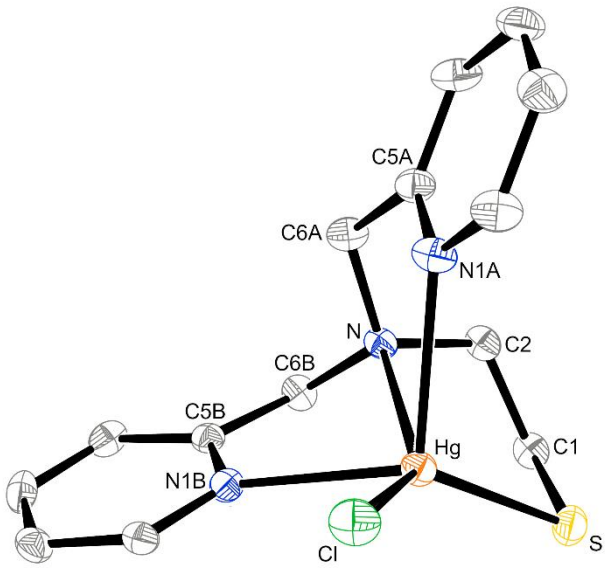

Figure 4. Thermal ellipsoid (50% probability) structure of **2**. Hydrogen atoms are omitted.

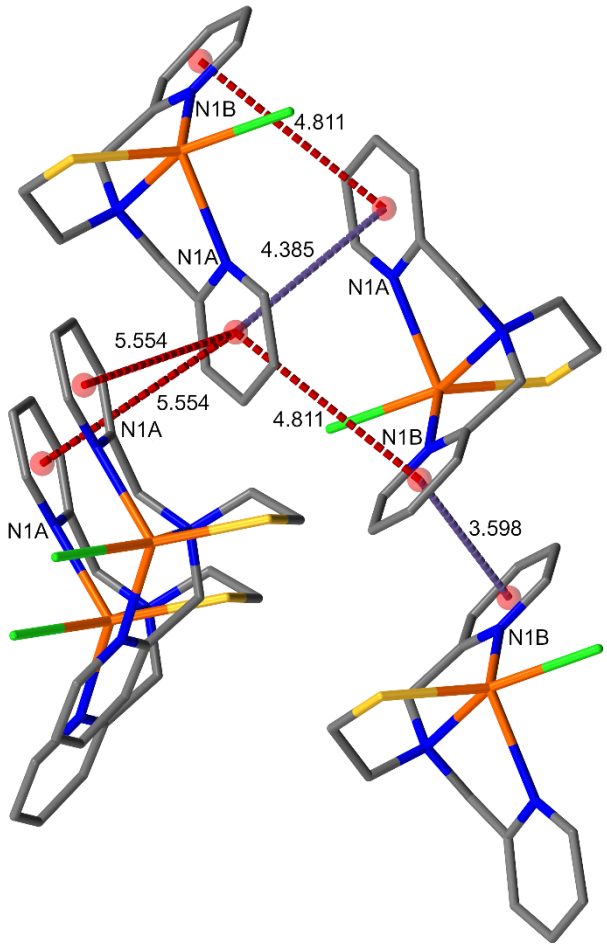

Figure 5. Intermolecular aromatic distances (Å) between pyridyl rings, identified by their nitrogen atoms, in **2**. Hydrogen atoms are omitted for clarity. Offset parallel pyridyl-pyridyl centroid distances in violet; multimolecular pyridyl centroid distances in red.

0.44)[53] with predominantly square pyramidal character. For the nominally axial pyridyl nitrogen N1A the bond distance to the metal center (2.510(4) Å) is slightly longer than its nominally equatorial counterpart N1B (2.480(3) Å) (Table 4). The Hg–N bond distance to the tripodal amine nitrogen is longer (2.644(3) Å) than the Hg–N bonds to both pyridyl nitrogens as observed in **1**·benzene. The N1A chelate ring has an envelope conformation with the methylene carbons in the flap positions. Both the N1B and S chelate ring have a half chair conformation. The mercury is within 0.280 Å of the N–N1B–Cl– S square plane. The supramolecular structure of **2** is extensively stabilized through interactions between aromatic rings (Fig. 5). Both pyridyl rings undergo OFF with their counterparts in inversion related neighboring molecules. In addition, EF interactions occur between the N1A and N1B pyridyls of neighboring inversion related molecules. These interactions form continuous chains of the complex along the *a* cell axis (Fig. S2). These chains are linked into a three-dimensional network through EF interactions between the N1A pyridyls that extend along a two-fold screw axes forming a zig-zag aryl embrace.[52]

Structural Comparison of Group 12 [MLCl]$_n$ Complexes

Known complex [Zn**L**Cl] (**3**)[45] crystallized in $P2_1/c$ as an isomorph of **2**. Although **3** has a predominantly trigonal bipyramidal structure ($\tau = 0.82$)[53], it overlays well with the structure of **2** (Fig. 6) and has a similar network of aromatic interactions (Fig. S3). Consistent with the smaller ionic radius of Zn^{2+}, the metal ligand bond distances in **3** are all shorter than those in **1** and **2**. The N–M–Cl bond angle is the largest around the metal ion in all three complexes and closest to the ideal value of 180° in **3**. The S–M–Cl bond angle is larger than the 90° ideal for all three complexes and the only metal–ligand bond angle that increases as the metal ion gets larger.

Structural comparisons to other complexes of L

Besides [Zn**L**Cl], only five structurally characterized complexes of **L** have been previously reported. The only dinuclear complex was $[Cu\mathbf{L}]_2(ClO_4)_2$,[54] in which the metal ions have distorted square pyramidal coordination geometry and the bridging

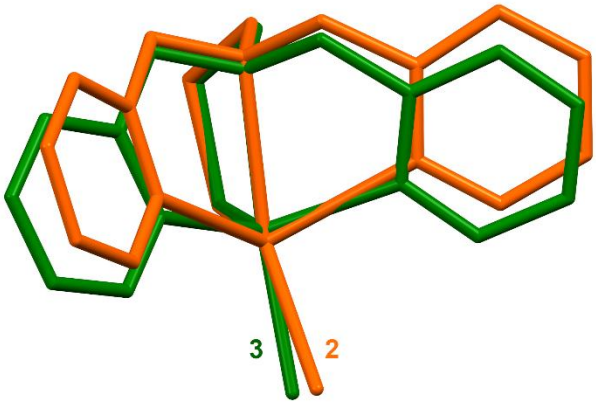

Figure 6. Overlay diagram (N_{am}–M–S) for isomorphs **2** and **3**.

$(CuS)_2$ is strongly puckered. The mononuclear complexes $[CoL(NCS)_2]$[55] and $[ReL(CO)_3]$[56] both have octahedral coordination geometry. In the Co^{3+} complex, the three nitrogen atoms of the tetradentate ligand are bound in a meridional fashion with the ligand sulfur atom joining two thiocyanate nitrogen atoms in the orthogonal direction. In contrast, the other mononuclear octahedral complex has a fac-$\{Re(CO)_3^+$ core restricting the ligand to facial tridentate coordination resulting in a pendant pyridyl ring that is in slow exchange with the bound pyridyl ring on the ^{13}C chemical shift time scale. Finally, the metallothionein-like trinuclear complexes $[CdL]_3(ClO_4)_3$ and $[ZnL]_3(ClO_4)_3{\cdot}4\ CH_3CN$ were recently reported, the first structurally characterized aggregates of group 12 metal ions with monocyclic M_3S_3 cores in the absence of a protein.[9] These complexes had predominantly trigonal bipyramidal metal coordination geometry ($\tau > 0.85$).[53] The rich variety of ligand coordination modes and aggregation states potentially available to complexes of L^- emphasizes the importance of complementing crystallographic characterization of low solubility compounds with additional studies to help clarify speciation when potentially pertinent.

Proton NMR of 1 and 2

Proton NMR spectra were obtained for both **1** (benzene removed from **1**·benzene in vacuo; nominally 50 µM–saturated (<2 mM)) and **2** (nominally 0.6–5.0 mM) in CD_3CN solutions over the temperature range −40 °C to 60 °C. Correlations between solid-state structures and solution-state spectroscopy are rarely definitive for group 12 metal ion complexes due to intramolecular reorganization, intermolecular exchange and variable oligomerization.[9, 57, 58] However, spectral changes with temperature and concentration were informative.

The four pyridyl protons of **1** and **2** have four well resolved resonances with similar chemical shifts for the two complexes ($\Delta\delta \leq$ 0.10 ppm; Fig. 7). These resonances exhibit only a modest linear dependence on temperature and negligible changes with concentration (data not shown). Three pyridyl protons (H_a, H_b, and H_c) are observed at higher chemical shift than **LH** for both complexes, consistent with the deshielding influence of metal ion binding. In contrast, H_d appears at lower chemical shift than **LH** in the complexes. Significantly, base broadening of the H_a peaks of **1** (at and below 20 °C) and **2** (at –40 °C) in CD_3CN is consistent with incompletely resolved heteronuclear coupling to the metal ions supporting slow metal-ligand exchange on the M–^{1}H coupling constant time scale (Fig. 7). Recall that the pyridyl rings of **1**·benzene have structurally distinct locations in the solid-state, trans from either the intraligand or bridging thiolate, which are conceivably magnetically inequivalent. Magnetic equivalence of the pyridyl protons of **1** can be explained by coincidentally identical chemical shifts as observed for $[Re(CO)_3L]$, which has one pendant and one bound pyridyl ring in the solid state,[56] or the coordinative malleability of the d^{10} metal ion allowing for rapid intramolecular exchange of the thiolate positions in the Cd_2S_2 ring without bond cleavage (Fig. 8). A related explanation is that the dimeric $[CdLCl]_2$ species is rapidly exchanging with other aggregates or becoming a monomeric species,

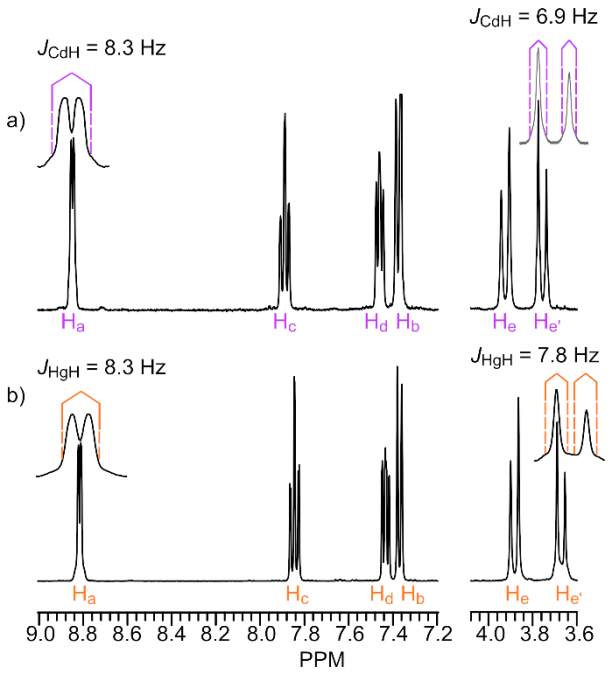

Figure 7. ^{1}H NMR highlights (CD_3CN, nominally 2 mM, –40 °C) for a) $[CdLCl]_2$·benzene (1·benzene) and b) [HgLCl] (2). Heteronuclear $J(^{111/113}Cd^1H)$ and $J(^{199}Hg^1H)$ couplings are shown as insets (See also Fig. S3). Resonances for H_f and H_g between 2.66 and 2.90 ppm not shown.

although concentration dependent NMR experiments suggest the complex is predominantly dimeric at concentrations approaching saturation (see Fig. 9 and discussion below). Although complex **2** also has two unique pyridyls in the solid-state structure, pyridyl equivalence is expected for the mononuclear complex after removal of solid-state constraints through Berry pseudorotation.[59]

While the pyridyl protons of **1** and **2** have comparable nearly invariant chemical shifts and proton-proton coupling constants under all conditions examined, the aliphatic protons behave differently as a function of temperature. Two geminally coupled doublets are observed for the methylene protons of **1** in CD_3CN over the temperature range −40 °C to 20 °C for nominal concentrations above 1 mM (Fig. 7). The more upfield H_e

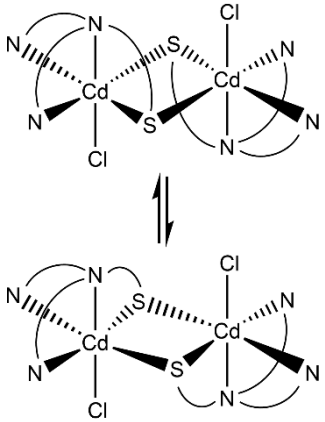

Figure 8. Proposed intramolecular twist for exchange of the thiolate positions in the Cd_2S_2 ring of **1** and associated cis and trans pyridyl environments.

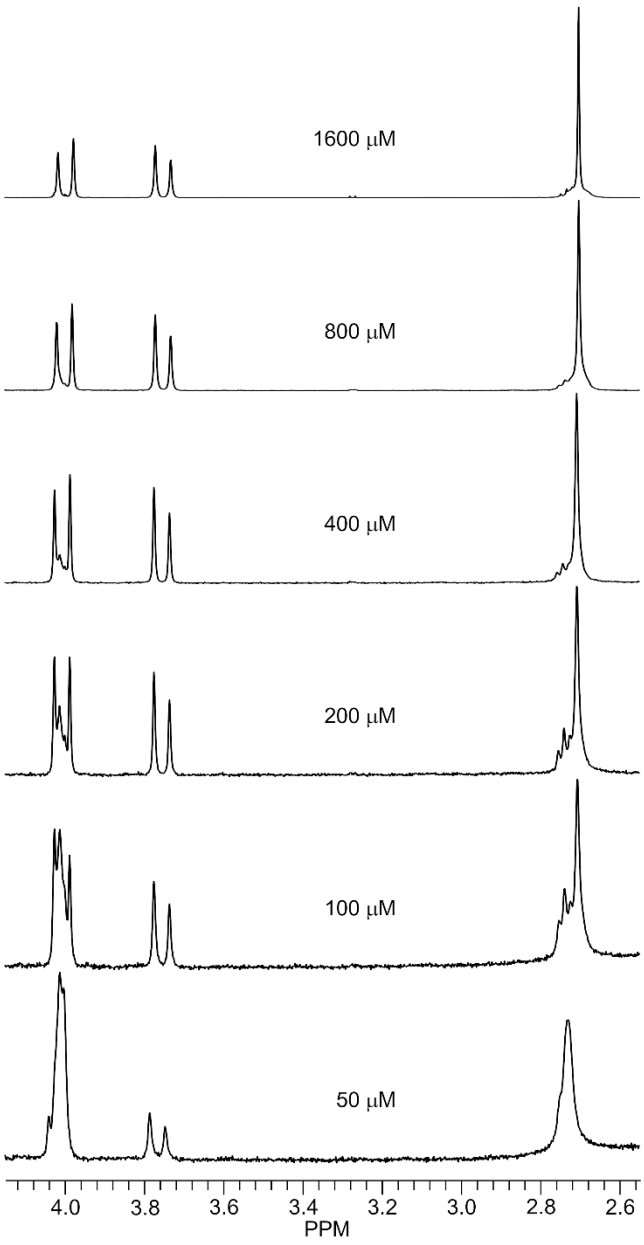

Figure 9. Methylene and ethylene proton resonances for **1** in CD_3CN solution at 20 °C as a function of nominal solution concentration.

protons also have partially resolved $J(^{111/113}Cd^1H)$ satellites under these conditions. As the concentration of **1** is lowered, these resonances lose intensity as a new singlet at δ 4.002 ppm grows in (Fig. 9). Simultaneously, the resonance at δ 2.702 ppm accounting for four ethylene protons is replaced by a broad multiplet at δ 2.731 ppm. The ethylene and methylene protons for two ligand environments are in slow exchange on the chemical shift time scale at 20 °C despite very small chemical shift differences. Dissociation of aggregate complexes to smaller complexes is mathematically predictable with dilution. Since a solvate of dimeric $[Cd\mathbf{L}Cl]_2$ was isolated at mM concentrations from MeOH/benzene, the prevalent species at high concentration in CD_3CN is assigned to the isolated dimer **1**. However, $\mathbf{L}^-$ is known to form higher aggregates, [9] which may

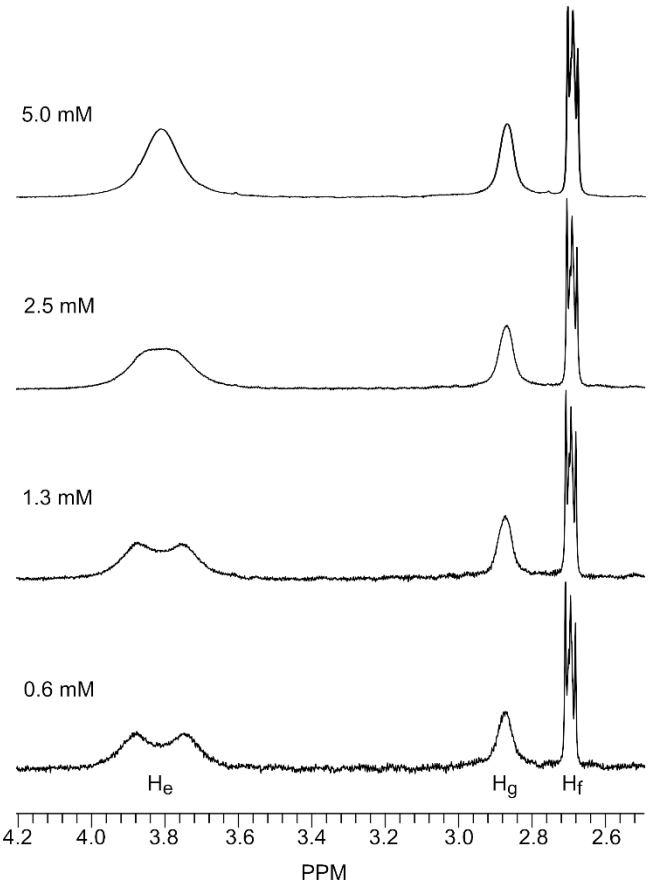

Figure 10. Methylene and ethylene proton resonances for **2** in CD_3CN solution at 20 °C as a function of nominal solution concentration.

be indistinguishable from **1** by proton NMR due to limited chemical shift dispersion. Limited solubility made ^{13}C NMR studies impractical. The species prevalent at low concentration is assigned to $[Cd\mathbf{L}Cl]$ since partial geminal resolution of the H_e protons was observed under cryogenic conditions (data not shown) and free ligand would be expected to have significantly different chemical shifts.

In contrast, the solution behavior of **2** suggests a monomer-dimer equilibrium strongly favoring monomeric $[Hg\mathbf{L}Cl]$ in acetonitrile under comparable conditions. The prevalence of a monomeric complex is supported by the broadened singlet for the methylene protons of **2** achieving partial geminal resolution upon dilution at 20 °C (Fig. 10). Dilution both shifts monomer-dimer equilibria towards the monomer and reduces collision rates, contributing to conditions which are more favorable for detecting coupling. Slow exchange conditions on the $J(^{199}Hg^1H)$, $^2J(^1H^1H)$ and chemical shift time scale were achieved by cooling a CD_3CN solution of **2** to −40 °C (Figs. 7, 11 and S4). The ethylene protons of **2** give rise to distinct resonances for H_f and H_g at all temperatures while the ethylene protons of **1** require cryogenic temperatures to be resolved into separate multiplets in CD_3CN. The chemical shift for H_f of **2** is minimally affected by temperature, but its vicinal coupling pattern is temperature dependent, and a low intensity downfield shoulder resonance is observed under cryogenic conditions at elevated

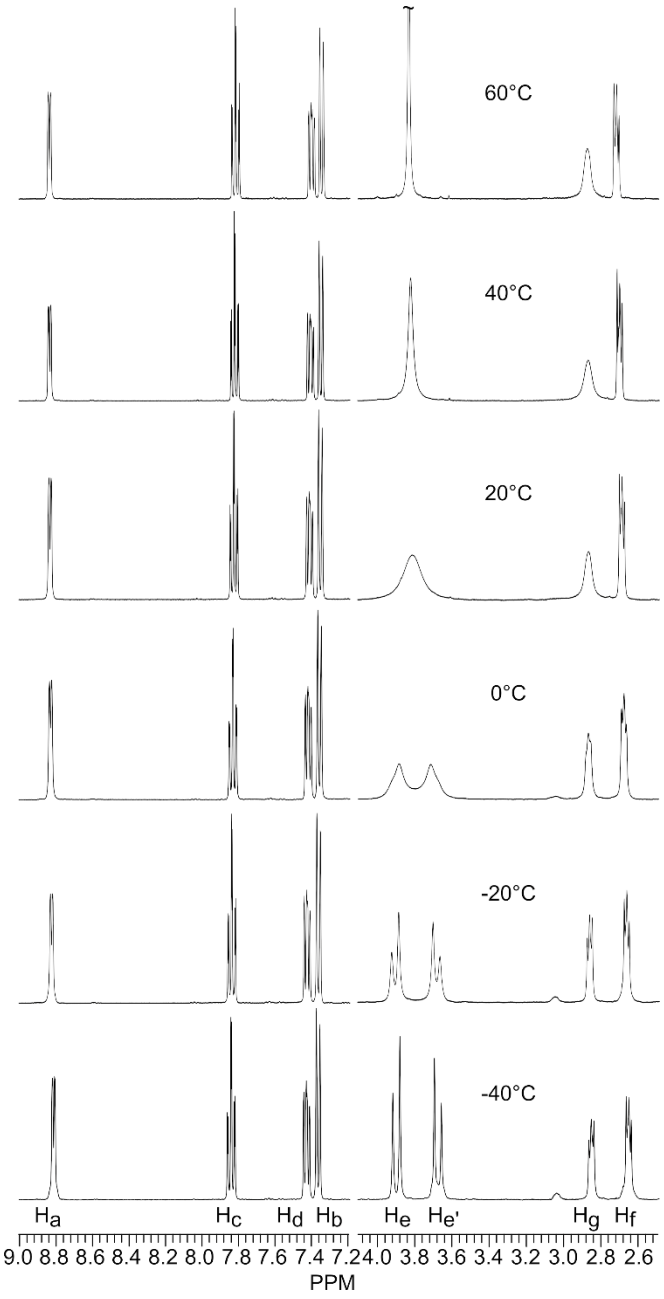

Figure 11. Ligand proton resonances for **2** (CD_3CN, nominally 5 mM) as a function of temperature. An expanded version of the ethylene proton region is provided in Fig. S4. An overlay of the H_a resonances at 60 °C and –40 °C accentuating the partially resolved $J(^{199}Hg^1H)$ satellites is provided in Fig. S3.

concentrations (Fig. S5). Furthermore, at higher concentrations the broad singlet for H_g at elevated temperatures resolves into upfield major and downfield minor (12% for 5 mM **2** at –40 °C Fig. 11) peaks with Δδ 0.18 ppm as the temperature is lowered. Significantly, geminal coupling of the H_e protons appears to resolve simultaneously with slow exchange of the H_f and H_g environments. Since the H_g protons are closest to the dimer interface, their chemical shift is expected to be impacted more by dimerization than other ligand protons as observed for **2**. Detailed NMR studies of additional series of group 12 complexes with $N_x^A S_y^-$ ligands under slow exchange conditions are needed to better understand the relationship between the chemical shifts of methylene protons adjacent to thiolates in Cd^{2+} and Hg^{2+} complexes and aggregation state.

The observed NMR behaviors for **2** can be explained by transient formation of μ-thiolato-bridged dimer **4** (Fig. 12), which may either dissociate to monomers, undergo M_2S_2 ring closure or liberate a pyridyl nitrogen from the coordination sphere of one metal to allow inversion of the central amine. We hypothesize that the exothermicity of forming the bridging M–S bond provides the energy needed to break a pyridyl M–N bond and make a dimer with two five coordinate metal atoms (**5**). The proposed mechanism is supported by the base broadening of the H_a resonance associated with J_{HgH} satellites in the NMR spectrum of **2** only being observed under conditions in which the geminal coupling of H_e is fully resolved (Fig. 11). Coincident ^1H chemical shifts for all four pyridyl protons of **L** under conditions in which monomeric and various dimeric metal complexes coexist is somewhat surprising, but precedented by the shared chemical shifts for pendant and bound pyridyl ring protons in [Re**L**$(CO)_3$].[56] Significantly, while a variety of mercury complexes with Hg_2S_2 rings have been structurally characterized,[7] they all have a metal coordination number of four except for one very sterically hindered complex with a coordination number of six.[60] In contrast, isolated complexes with Cd_2S_2 rings predominantly have a metal coordination number of six.[7]

In summary, readily available 1D NMR methods have been used to show that the aggregation states of group 12 [M**L**Cl]$_n$ complexes are concentration dependent in the μM–mM range. For the group 12 complexes of **L** investigated, the aggregation state of isolated X-ray quality crystals isolated are consistent

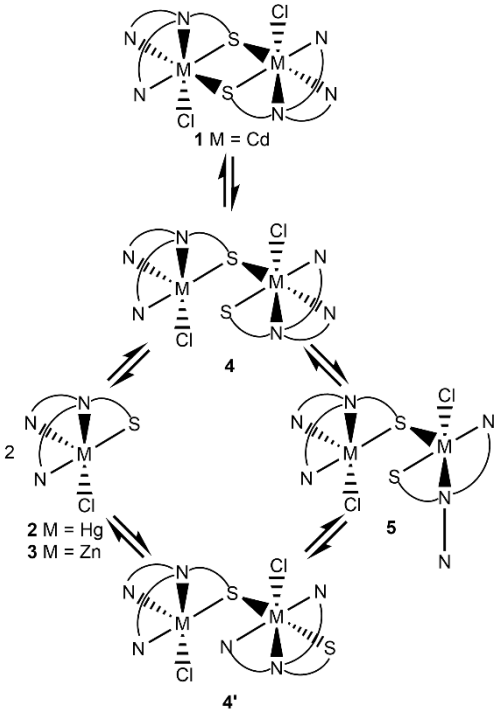

Figure 12. Proposed reaction mechanism for exchanging methylene protons and interconverting monomeric and dimeric complexes of **L**.

with concentration and temperature trends in ^{1}H NMR spectra. Trends in homonuclear and heteronuclear coupling constants were especially informative in the proton NMR studies.

ESI-MS of 1 and 2

Further investigations of **1** and **2** in acetonitrile solutions by direct infusion positive ion ESI-MS were used to demonstrate coexistence of mononuclear and dinuclear species in solution, as well as the fragmentation behavior of the dinuclear species. Conventionally, electrospray ionization is viewed as a very sensitive soft ionization technique well suited to qualitative characterization of a mixture of complex ions with different metal-to-ligand ratios. Observed ions were assigned by qualitative comparison of isotope patterns and analysis of collision-induced dissociation patterns. Since physicochemical properties can strongly impact ionization and transformations or fragmentations may occur inside the electrospray droplet preventing representative transfer from solution to gas phase,[61-63] quantitative correlations between ESI-MS and solution phase studies were not attempted.

The initial ESI-MS of **1** with a capillary temperature of 200 °C had $[Cd\mathbf{L}]^+$ as the base peak and the relative intensity of $[Cd_2\mathbf{L}_2Cl]^+$ was approximately 35% (data not shown). Lowering the capillary temperature to 100 °C provided $[Cd_2\mathbf{L}_2Cl]^+$ as the base peak (Fig. 13(a)), however the relative intensity of $[Cd\mathbf{L}]^+$ remained high (~75%) and there was also a significant amount of $[Cd_3\mathbf{L}_3Cl_2]^+$ present (~33%). In contrast, at the lower capillary temperature the ESI-MS of **2** had $[Hg\mathbf{L}]^+$ as the base peak and a modest 17% relative intensity of $[Hg_2\mathbf{L}_2Cl]^+$ and no detectable $[Hg_3\mathbf{L}_3Cl_2]^+$ (Fig. 13(b)). Peak assignments were confirmed by comparison of ZoomScan spectra for mass-selected peaks with theoretical predictions (Fig. S6). The collision-induced fragmentation of both $[M_2\mathbf{L}_2Cl]^+$ ions proceeded with loss of $[M\mathbf{L}Cl]$ to produce $[M\mathbf{L}]^+$ as observed for related clusters (Fig. 14).[9] The $[Cd_3\mathbf{L}_3Cl_2]^+$ ions were not sufficiently stable in the ion trap for clean isolation. Interestingly, when examined under comparable conditions, $[Hg_2\mathbf{L}_2Cl]^+$ fragmented at approximately 60% of the collision energy required to fragment $[Cd_2\mathbf{L}_2Cl]^+$. The

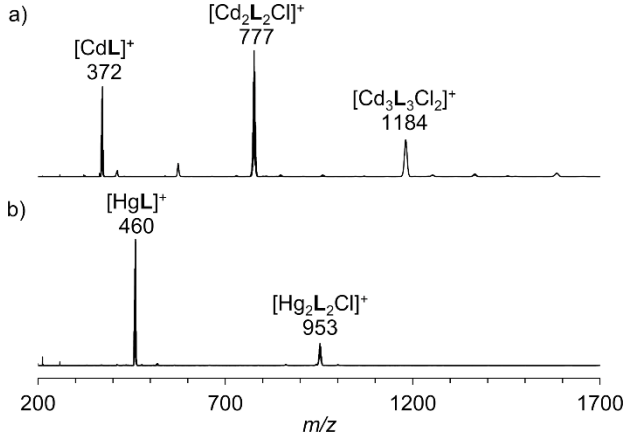

Figure 13. Direct infusion positive-mode ESI-MS of acetonitrile solutions of nominally 0.5 mM (a) **1** and (b) **2** with predicted maximum intensity isotopomer of assigned ions indicated.

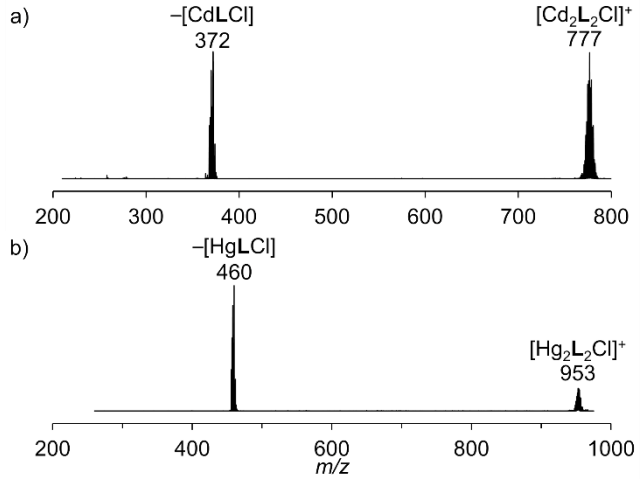

Figure 14. Collision-induced fragmentation pattern for mass-selected (a) $[Cd_2\mathbf{L}_2X]^+$ (777 ± 17) at 13% collision energy and (a) $[Hg_2\mathbf{L}_2X]^+$ (953 ± 20) at 8% collision energy. Peaks identified by predicted maximum intensity isotopomer of assigned ions.

ESI-MS studies of **1** and **2** complement the solution NMR studies by demonstrating higher stability for the dinuclear ions of Cd^{2+} than Hg^{2+} in the gas phase. Note, however, that individual mass spectra do not provide structural information permitting distinction between cyclic and acyclic M_nS_n core structures.

Conclusions

New chloride complexes of Cd^{2+} and Hg^{2+} with the deprotonated N_3S donor ligand 2-[bis(2-pyridinylmethyl)amino]ethanethiol (**LH**) were synthesized and characterized in the both the solid state and solution state for comparison with the known complex $[Zn\mathbf{L}Cl]$.[45] The dinuclear cadmium complex crystallized as $[Cd\mathbf{L}Cl]_2$·benzene in the triclinic space group *P*-1 with a distorted octahedral Cd^{2+} coordination geometry. The two metal centers of the dimeric complex are bridged by ligand thiolate groups. Mononuclear $[Hg\mathbf{L}Cl]$ crystallized in the monoclinic space group $P2_1/c$ with predominantly square pyramidal geometry as an isomorph of the predominantly trigonal bipyramidal $[Zn\mathbf{L}Cl]$ complex. Trends in variable temperature and variable concentration proton NMR studies of **1** and **2** suggested two metal-bound **L** species were prevalent in solution. These were assigned to $[M\mathbf{L}Cl]$ and $[M\mathbf{L}Cl]_2$. Direct infusion ESI-MS studies confirmed coexistence of mononuclear and dinuclear metal ion complexes in acetonitrile solution. Previously, a monomer-dimer equilibrium was used to rationalize the concentration dependence of $[Zn\mathbf{L}Cl]$ hydrolytic activity.[45] This work emphasizes the importance of considering potential variations and differences in oligomerization of group 12 metal ion complexes as a function of concentration when working with thiolate ligands. Furthermore, the feasibility of using readily available one-dimensional proton NMR techniques paired with direct infusion ESI-MS methods to investigate oligomerization of group 12 metal ion thiolate complexes has been documented.

Author Contributions

Michelle A. Sturner: Investigation, Methodology, Validation, Visualization, Writing – Original Draft. Isla D. Thomas: Investigation, Methodology. Joshua E. Owusu-Koramoah: Investigation, Validation. Todd M. Reynolds: Investigation, Validation, Formal analysis, Data curation. Steven M. Berry: Investigation, Methodology, Writing – Editing. Raymond J. Butcher: Data curation, Formal analysis. Deborah C. Bebout: Project administration, Supervision, Investigation, Methodology, Visualization, Writing – Review & Editing.

Conflicts of interest

There are no conflicts to declare.

Acknowledgements

The authors thank both the National Science Foundation (0750119) and the Petroleum Research Fund for funding initial aspects of this research. We also thank the Camille and Henry Dreyfus Foundation for a Scholar Fellow Award to D.C.B. (SF-02-006) for support of S.M.B and the research. In addition, we are grateful for William & Mary funding of undergraduate participation and the research. Purchases of the William & Mary SMART Apex II diffractometer and Agilent 400-MR D2 NMR spectrometer were supported by the National Science Foundation (0443345 and 1337295, respectively), as well as William & Mary. We also acknowledge John C. Poutsma for providing access to research instrumentation for the ESI-MS studies.

References

1 R. Friedman, *Dalton Trans.,* 2014, **43**, 2878-2887.
2 S. V. Razin, V. V. Borunova, O. G. Maksimenko and O. L. Kantidze, *Biochem. (Mosc.),* 2012, **77**, 217-226.
3 M. Perinelli, M. Tegoni and E. Freisinger, *Inorg. Chem.,* 2020, **59**, 16988-16997.
4 W. M. Matousek and A. T. Alexandrescu, Biochim. Biophys. Acta, Proteins and Proteomics, 2004, 1702, 163-171.
5 M. Wiedmann, P. K. Dranchak, M. Aitha, B. Queme, C. D. Collmus, M. M. Kashipathy, L. Kanter, L. Lamy, J. M. Rogers, D. Tao, K. P. Battaile, G. Rai, S. Lovell, H. Suga and J. Inglese, J. Biol. Chem., 2021, 296, 100628.
6 6 V. Alterio, E. Langella, G. De Simone and S. M. Monti, Mar. Drugs, 2015, 13, 1688-1697.
7 Cambridge Structural Database, 2023, version 5.44.
8 W. Lai, S. M. Berry, W. P. Kaplan, M. S. Hain, J. C. Poutsma, R. J. Butcher, R. D. Pike and D. C. Bebout, *Inorg. Chem.,* 2013, **52**, 2286-2288.
9 H. M. Brennan, S. G. Bunde, Q. Kuang, T. V. Palomino, J. S. Sacks, S. M. Berry, R. J. Butcher, J. C. Poutsma, R. D. Pike and D. C. Bebout, *Inorg. Chem.,* 2022, **62**, 19857-19869.
10 J. A. Viehweg, S. M. Stamps, J. J. Dertinger, R. L. Green, K. E. Harris, R. J. Butcher, E. J. Andriole, J. C. Poutsma, S. M. Berry and D. C. Bebout, *Dalton Trans.,* 2010, **39**, 3174-3176.
11 M. R. Hallinger, A. C. Gerhard, M. D. Ritz, J. S. Sacks, J. C. Poutsma, R. D. Pike, L. Wojtas and D. C. Bebout, *ACS Omega,* 2017, **2**, 6391-6404.
12 L. Pecs, J. Ozols, A. Kemme, J. Bleidelis and A. Sturis, *Latv. PSR Zinat. Akad. Vestis, Kim. Ser.,* 1979, 259-264.
13 L. Pecs, V. S. Fundamenskii, O. G. Matyukhina, J. Ozols, A. Sturis and Y. A. Bankovskii, *Koord. Khim.,* 1984, **10**, 1427-1430.
14 O. G. Matyukhina, A. N. Sobolev, L. Pecs, J. Leejs, J. Ozols and Y. A. Bankovskii, *Zh. Strukt. Khim.,* 1985, **26**, 113-118.
15 O. G. Matyukhina, A. N. Sobolev, I. Berzina, J. Asaks and Y. A. Bankovskii, *Koord. Khim.,* 1985, **11**, 822-825.
16 L. Pech, Y. Bankovskii, I. Berzina, V. Be'skii, A. Sobolev and J. Ashaks, *Latv. Kim. Z.,* 1997, 87-88.
17 O. G. Matyukhina, J. Ozols, A. N. Sobolev, J. Lejejs and Y. A. Bankovskii, *Latv. PSR Zinat. Akad. Vestis, Kim. Ser.,* 1983, 672-677.
18 I. R. Berzinya, V. K. Bel'skii, Y. K. Ozols and A. P. Sturis, *Latv. PSR Zinat. Akad. Vestis, Khim. Ser.,* 1984, 52.
19 E. Silina, V. Belsky, V. Zavodnik, L. Pech and D. Zaruma, *Latv. Kim. Z.,* 2006, 292-294.
20 R. A. Santos, E. S. Gruff, S. A. Koch and G. S. Harbison, *J. Am. Chem. Soc.,* 1991, **113**, 469-475.
21 M. Bochmann, K. J. Webb and A. K. Powell, *Polyhedron,* 1992, **11**, 513-516.
22 J. Otto, I. Jolk, T. Viland, R. Wonnemann and B. Krebs, *Inorg. Chim. Acta,* 1999, **285**, 262-268.
23 W. Sun, L. Zhang and K. Yu, *J. Chem. Soc., Dalton Trans.,* 1999, 795-798.
24 W. F. Wacholtz and J. T. Mague, *Acta Crystallogr. Sect. C: Cryst. Struct. Commun.,* 2001, **C57**, 1400-1402.
25 M. T. Ng, T. C. Deivaraj and J. J. Vittal, *Main Group Met. Chem.,* 2002, **25**, 581-582.
26 X. Tang, R. Yuan, Z. Ren, H. Li, Y. Zhang and J. Lang, *Inorg. Chem.,* 2009, **48**, 2639-2651.
27 X. Tang, H. Yu, B. Gao and J. Lang, *Dalton Trans.,* 2017, **46**, 14724-14727.
28 A. Zheng, H. Wang, C. Lü, Z. Ren, H. Li and J. Lang, *Dalton Trans.,* 2012, **41**, 558-566.
29 B. V. Cheesman, A. P. Arnold and D. L. Rabenstein, *J. Am. Chem. Soc.,* 1988, **110**, 6359-6364.
30 W. Maret and Y. Li, *Chem. Rev.,* 2009, **109**, 4682-4707.
31 P. C. Sanghani, H. Robinson, W. F. Bosron and T. D. Hurley, *Biochemistry (N. Y.),* 2002, **41**, 10778-10786.
32 T. A. Pauly, J. L. Ekstrom, D. A. Beebe, B. Chrunyk, D. Cunningham, M. Griffor, A. Kamath, S. E. Lee, R. Madura and D. Mcguire, *Structure,* 2003, **11**, 1071-1085.
33 S. B. Long, P. J. Hancock, A. M. Kral, H. W. Hellinga and L. S. Beese, *Proc. Natl. Acad. Sci. U. S. A.,* 2001, **98**, 12948-12953.
34 E. Harjes, P. J. Gross, K. Chen, Y. Lu, K. Shindo, R. Nowarski, J. D. Gross, M. Kotler, R. S. Harris and H. Matsuo, *J. Mol. Biol.,* 2009, **389**, 819-832.
35 G. Auerbach, A. Herrmann, A. Bracher, G. Bader, M. Gütlich, M. Fischer, M. Neukamm, M. Garrido-Franco, J. Richardson and H. Nar, *Proc. Natl. Acad. Sci. U. S. A.,* 2000, **97**, 13567-13572.
36 P. Fang, X. Yu, S. J. Jeong, A. Mirando, K. Chen, X. Chen, S. Kim, C. S. Francklyn and M. Guo, *Nat. Commun,* 2015, **6**, 6402.
37 N. J. Pace and E. Weerapana, *Biomolecules,* 2014, **4**, 419-434.
38 38 E. Baraldi, K. D. Carugo, M. Hyvönen, P. L. Surdo, A. M. Riley, B. V. L. Potter, R. O'Brien, J. E. Ladbury and M. Saraste, *Structure,* 1999, **7**, 449-460.
39 T. A. Leonard, B. Różycki, L. F. Saidi, G. Hummer and J. H. Hurley, *Cell,* 2011, **144**, 55-66.
40 Y. Tong, W. Tempel, L. Nedyalkova, F. MacKenzie and H. Park, *PLOS ONE,* 2009, **4**, e7165.
41 D. C. Tully, H. Liu, A. K. Chatterjee, P. B. Alper, R. Epple, J. A. Williams, M. J. Roberts, D. H. Woodmansee, B. T. Masick and C. Tumanut, *Bioorg. Med. Chem. Lett.,* 2006, **16**, 5112-5117.
42 D. Frey, O. Braun, C. Briand, M. Vašák and M. G. Grütter, *Structure,* 2006, **14**, 901-911.
43 S. Eustermann, C. Brockmann, P. V. Mehrotra, J. Yang, D. Loakes, S. C. West, I. Ahel and D. Neuhaus, *Nat. Struct. Mol. Biol.,* 2010, **17**, 241-243.

44 M. Bijlmakers, J. M. C. Teixeira, R. Boer, M. Mayzel, P. Puig-Sàrries, G. Karlsson, M. Coll, M. Pons and B. Crosas, *Sci. Rep.,* 2016, **6**, 29232.
45 H. Kurosaki, T. Tawada, S. Kawasoe, Y. Ohashi and M. Goto, *Bioorg. Med. Chem. Lett.,* 2000, **10**, 1333-1337.
46 H. Kurosaki, T. Tawada, S. Kawasoe, Y. Ohashi and M. Goto, *Anal. Sci. : X-Ray Struct. Anal. Online,* 2003, **19**, x27-x28.
47 S. Itoh, M. Nagagawa and S. Fukuzumi, *J. Am. Chem. Soc.,* 2001, **123**, 4087-4088.
48 G. M. Sheldrick, *Acta Cryst. C,* 2015, **71**, 3-8.
49 L. Loots and L. J. Barbour, in *The Importance of Pi-Interactions in Crystal Engineering,* ed. ed. E. R. T. Tiekink and J. Zukerman-Schpector, John Wiley & Sons, Ltd, West Sussex, UK, 2012, pp.109-124.
50 C. Janiak, *J. Chem. Soc., Dalton Trans*., 2000, 3885-3896.
51 D. B. Ninković, G. V. Janjić and S. D. Zarić, *Cryst. Growth Des.,* 2012, **12**, 1060-1063.
52 I. Dance and M. Scudder, *CrystEngComm,* 2009, **11**, 2233-2247.
53 A. W. Addison, T. N. Rao, J. Reedijk, J. Van Rijn and G. C. Verschoor, *J. Chem. Soc., Dalton Trans.,* 1984, 1349-1356.
54 S. Itoh, M. Nagagawa and S. Fukuzumi, *J. Am. Chem. Soc.,* 2001, **123**, 4087-4088.
55 F. Jiang, M. A. Siegler, X. Sun, L. Jiang, C. Fonseca Guerra and E. Bouwman, *Inorg. Chem.,* 2018, **57**, 8796-8805.
56 N. Lazarova, J. Babich, J. Valliant, P. Schaffer, S. James and J. Zubieta, *Inorg. Chem.,* 2005, **44**, 6763-6770.
57 D. C. Bebout, D. E. Ehmann, J. C. Trinidad, K. K. Crahan, M. E. Kastner and D. Parrish, *Inorg. Chem.,* 1997, **36**, 4257-4264.
58 D. C. Bebout, J. F. Bush II, K. K. Crahan, M. E. Kastner and D. A. Parrish, *Inorg. Chem.,* 1998, **37**, 4641-4646.
59 R. S. Berry, *J. Chem. Phys.,* 2004, **32**, 933-938.
60 H. Akdas, E. Graf, M. W. Hosseini, A. De Cian, A. Bilyk, B. W. Skelton, G. A. Koutsantonis, I. Murray, J. M. Harrowfield and A. H. White, *Chem. Commun.,* 2002, , 1042-1043.
61 M. C. Kuprowski and L. Konermann, *Anal. Chem.,* 2007, **79**, 2499-2506.
62 M. Peschke, U. H. Verkerk and P. Kebarle, *J. Am. Soc. Mass Spectrom.,* 2004, **15**, 1424-1434.
63 N. B. Cech and C. G. Enke, *Mass Spectrom. Rev.,* 2001, **20**, 362-387.